PROGRESS ON THE IPNS ENRICHED URANIUM BOOSTER TARGET*

CONF-8609234--1

A. E. Knox, J. M. Carpenter, J. L. Bailey,

R. J. Armani, R. N. Blomquist, B. S. Brown,

D. R. Henley, A. G. Hins, B. A. Loomis,

A. W. Schulke and H. R. Thresh

CONF-8609234--1

DE87 004846

Argonne National Laboratory
Argonne, Illinois 60439 USA

ABSTRACT

We describe the Enriched Uranium Booster Target designed for use in Argonne's Intense Pulsed Neutron Source. This report contains a general description of the system, and descriptions of the thermal-hydraulic and loss-of-coolant accident analyses, of the neutronic, criticality and power density calculations, of the assessment of radiation and thermal cycling growth, and of the disk fabrication methods. We also describe the calculations of radionuclide buildup and the related hazards analysis and our calculations of the temperature and stress profiles in the disks, and briefly allude to considerations of security and safeguards.

I. Introduction

The purpose of the Enriched Uranium Booster Target (the "Booster") is to increase the intensity of the neutron beams from IPNS. Conceived in 1980, the design project began in earnest three years ago. We took the design-limiting constraints to be the maximum power (about 100. kW) that could be dissipated by the existing cooling system without major modification and with the maximum-envisionable current delivered by the Rapid Cycling Synchrotron, and the space restrictions of the existing moderator, reflector, target-

*Work supported by the U.S. Department of Energy

handling and beam port arrangements, consistent with safety and security requirements. We described our progress up to about a year ago in an earlier report.[1]

The final design consists of a set of Zircaloy-2-clad, 77.5% ^{235}U enriched alloy disks of the same constitution as the present, depleted-Uranium target,[1] cooled by H_2O, and decoupled from the immediate surroundings by a layer of newly-developed ^{10}Boron-Copper composite material to provide a short prompt-neutron generation time and thus preserve a short response time. The value of k_{eff} is .80 for this target in its operating surroundings. The heat to be dissipated is about 83.kW for a 20.μA, 500. MeV beam, the maximum proton beam power envisionable. (With the present target, the thermal power is about 10. kW for a 15 μA, 450 MeV beam.) The expected gain in neutron beam intensity for the same proton beam conditions is a factor of about 3 (not $1/(1 - k_{eff}) = 5.$, because the proton-induced source neutrons are not all distributed in the $k_{eff} = .80$ mode and because the target-moderator coupling differs in the Booster case from the present case; furthermore because the depleted uranium target has a significant gain, $1/(1 - k_{eff}) = 1.1$). We expect that the fraction of neutrons which appear delayed will increase significantly from its present value of about 0.0044, to about 0.03, and are devising both hardware and software measures to cope with this in the instruments in which the increase is found significant. We further expect to have to make some local modifications to the main shielding and that of some of the scattering instruments. We have already installed two flowing liquid CH_4 moderators, operating at about 100.°K, that we believe will be suitable for the higher power target; we are constructing a new grooved, solid CH_4 moderator of improved design, for installation with the Booster.

Because the power density distribution is much broader in the multiplying booster target than in the depleted uranium target, disks need not be much thinner than those in the present target in spite of the much larger total power. We need 1/2-inch thick disks only in the front section of the target; the remainder are 1" thick. 304 stainless steel flow guides maintain 0.060" thick channels between disks for cooling. Eight disks chosen so as to provide the maximum amount of diagnostic information, contain a centered, stainless-steel-clad thermocouple located in a 1/16" diameter, Zircaloy-2 thermowell. The assembly of disks, compressed by concentric Inconel springs, rests in a welded vessel of 304 stainless steel. Flexible, corrugated, steel-braid-sheathed, stainless steel tubes carry cooling water to and from the target.

Alloying, casting, machining and Hot Isostatic Pressure bonding of the target disks has been done under contract at the Oak Ridge Y-12 facility, using processes similar to those developed at Argonne for producing the present depleted Uranium target disks. Differences in the casting processes have led to a somewhat-less-desirable metallurgical state of the Booster uranium, than that of the material of the present target. Figure 1 shows the Booster target located in the moderator/reflector assembly.

The cooling system is essentially the same as has been in use with the present target; we have joined the two identical systems, each of which previously cooled one of the two targets (the Radiation Effects Target, no longer used but still available, and the Neutron Scattering Target), for parallel, simultaneous operation to cool the Booster. To provide for removal of the substantial fission product decay heat in the event of loss of the primary cooling system, we have installed a low-capacity backup cooling system operated from two battery-supplied uninterruptable power sources. Other minor modifications have made it possible to backfit for D_2O cooling if we find it necessary to shorten the Booster response time. As previously, the cooling systems lie in sealed, Helium-filled tanks, vented to the facility exhaust, which is continuously monitored for radiation. Each circuit contains filters, heat exchangers, surge tanks, ion exchangers, flow and gross gamma radiation monitors as earlier. There is one fission product monitor. During operation, we will periodically remove cooling water, demineralizer resin and surge tank gas samples to monitor for abnormal radioactivity. This remains our method for sensing clad integrity and provides a criterion for continued target operation.

We have installed a somewhat upgraded system of instrumentation, controls and interlocks for use with the Booster. Figure 2 schematically shows the Booster Target cooling system.

We do not expect clad failure due to fatigue under cyclic thermal stress to limit the life of the target. Somewhat greater metallurgical texture in the Booster target material than in that of the present target, combined with greater burnup, will lead to somewhat anisotropic dimensional changes in the disks--at the time of writing we are assessing these effects, which we now believe will limit the target service lifetime to about five years.

The total costs (engineering and supporting studies, process development, fabrication and installation) amount to $1.5 M. We have used a computer-based PERT system to plan and control the project. Installation and first operation are expected in Fall of 1986. We have recorded slow neutron beam spectra from the moderators under what we hope will be reproducible

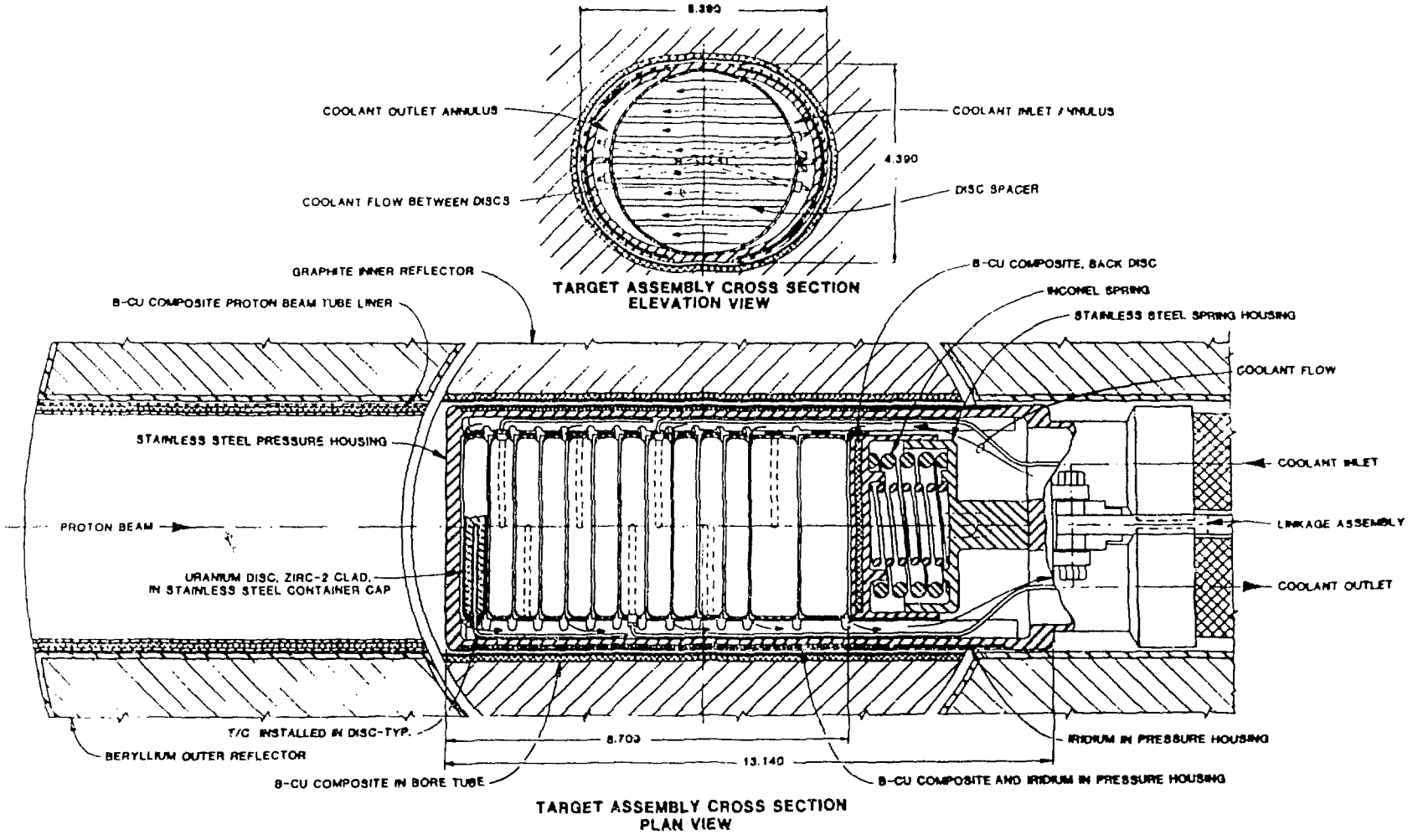

Fig. 1 Booster Target Installed in Moderator/Reflector Assembly

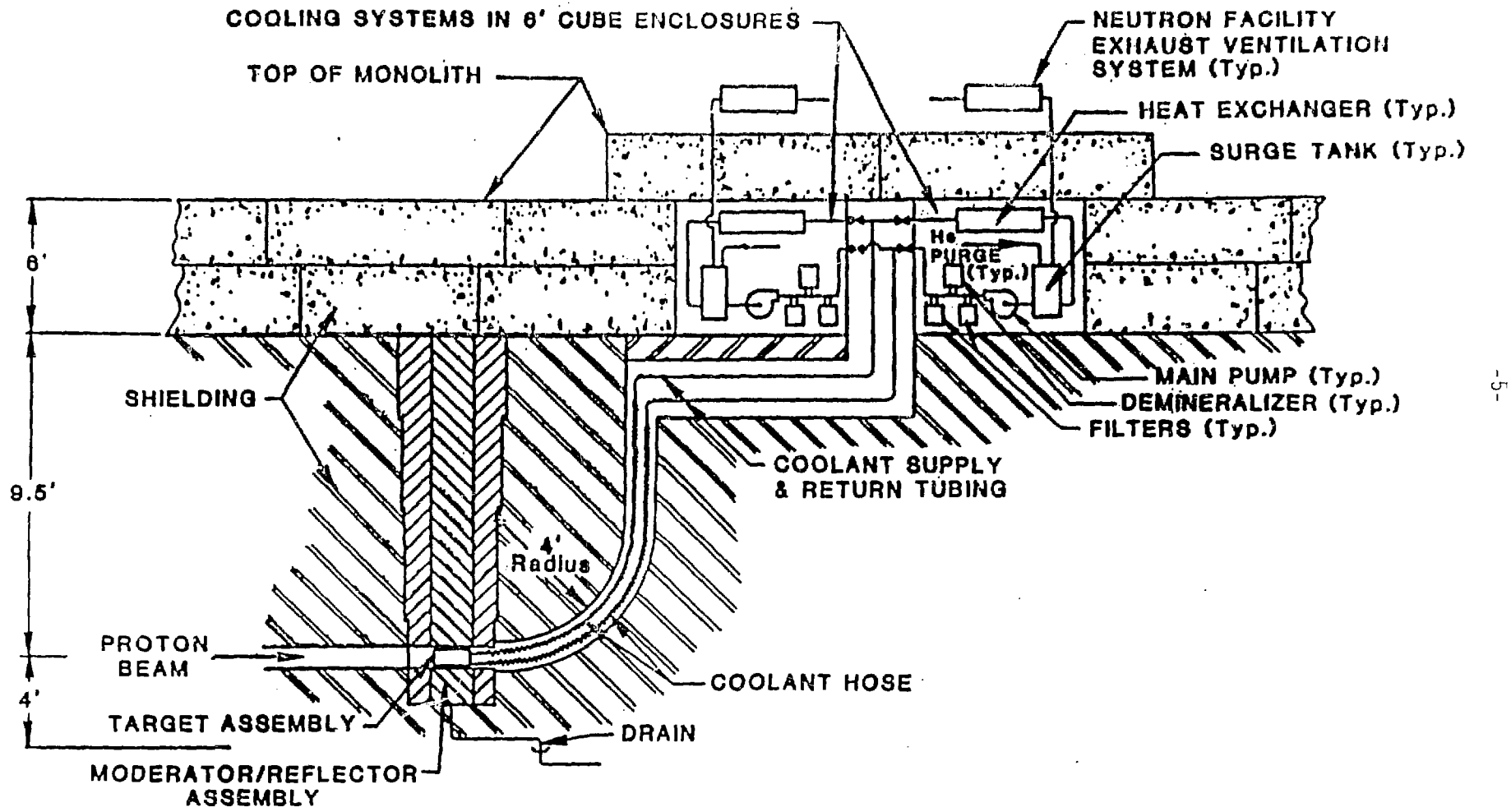

Fig. 2 Cross Section Elevation Through IPNS Facility

conditions prior to the end of operation of the present target, in preparation for relative intensity measurements after Booster installation.

II. Thermal-Hydraulic Analysis

Cooling System

The increased power in the Booster target requires twice the coolant flow of that in the present target; modifying the two existing, independent systems (Neutron Scattering Target and Radiation Effects Target) for parallel operation provides the required coolant flow. On the basis of field tests of a single system, we have developed a computer model[2] of the hydraulic behavior of the cooling system, with which we calculate the relationship between pressure differential and flow rate, the "performance curve", of the combined systems at the tee connections to the Booster target. Figure 3 shows this Cooling System Supply curve, which we have used in the course of hydraulic analysis to describe the interface between the cooling system and the target itself.

Field measurements have also provided the heat removal capacity of the existing heat exchangers; these tests indicate that the two heat exchangers together are adequate for the increased heat load of the Booster target. Table 1 gives the operating parameters of the cooling system.

Table 1

Operating Parameters of the Cooling System

Coolant	H_2O
Minimum coolant flow rate	90. gpm
Maximum coolant supply temperature	120. °F
Temperature Differential	6.5°F
Pressure Differential	18. psi

Booster Target Analysis

Coolant flows to and from the target through pipe connections made at the back (opposite the proton entry) end of the target (see Figure 1). Channeling in the back of the target housing directs flow to the inlet plenum and from the outlet plenum, which constitute the space between the round target disk caps and the elliptical vessel. When the disks and caps are assembled in the housing (they are compressed by coil springs located in the back of the vessel) slots in the face of each cap form parallel flow ducts

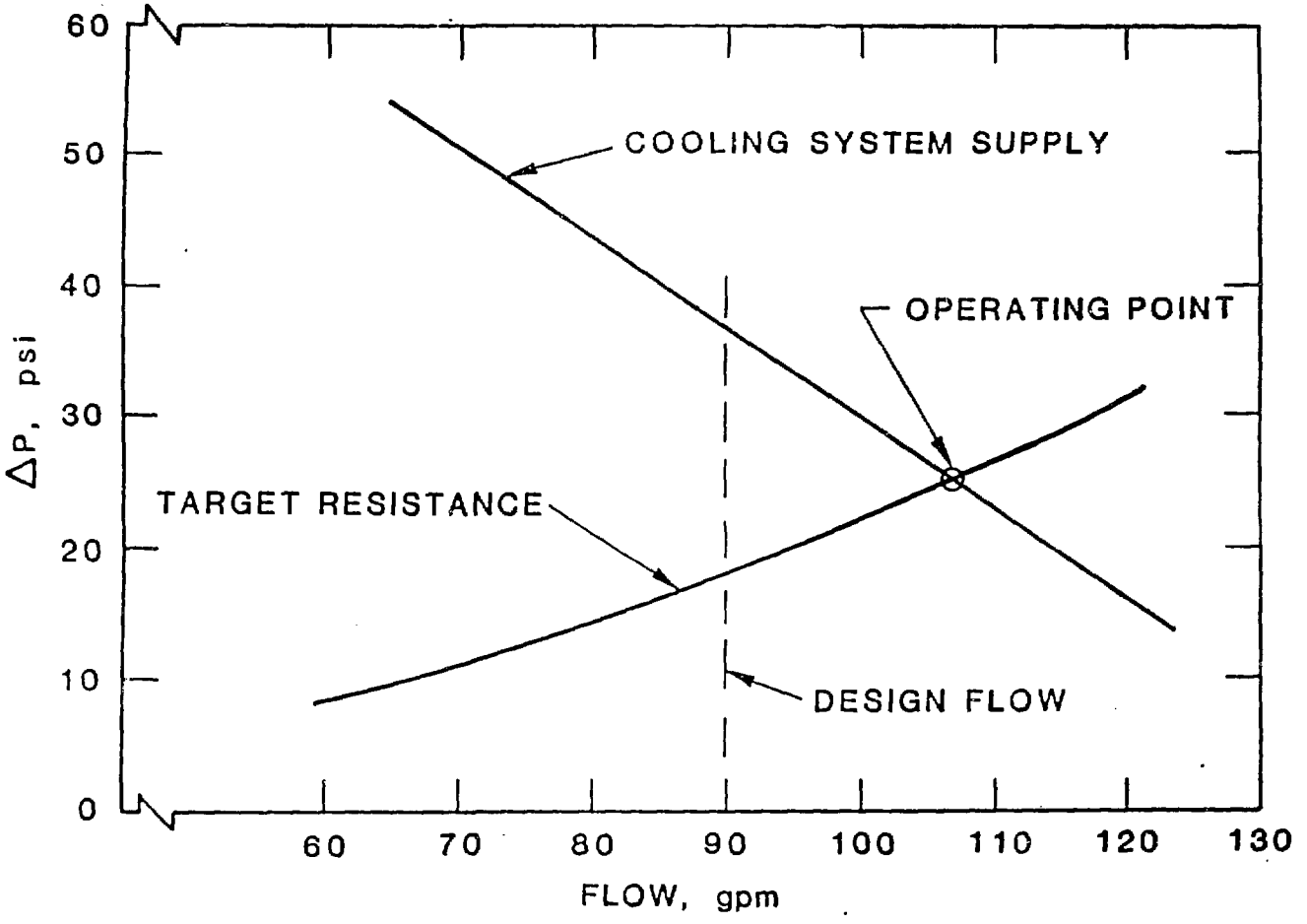

Fig. 3 Hydraulic Performance Curves for the Two Cooling Systems Operating in Parallel

connecting the inlet and outlet plenums. Forced convection in these ducts cools the faces of the disks. An accurate small-clearance fit between the caps and radial arcs machined in the housing walls prevents short circuiting of coolant past the caps.

The assembled target has 13 target disks and 14 flow channels. The front seven channels are full flow channels, and comprise three main slots and two cirumferential leakage paths; the seven channels in the back carry reduced flow on account of the lower local power density, and comprise eight main flow paths and two leakage paths.

A study by the general systems code SALT, using the Darcy equation with Kármán-Nikuradse friction factors and Crane's[3] entrance and exit loss coefficients to calculate pressure drops, has determined the pressure drops and the velocity and pressure profiles in the assembly, its associated hoses and piping up to the tee connections. Figure 4 schematically represents the computer model of the target. Using these results and the performance curve of the cooling system, we have developed a superimposed curve of the supply and resistance pressure differentials vs. flow rate. The performance curves indicate that at 90 gpm total flow rate, the two pumps operating in parallel produce a head well in excess of what is required (approximately 13 psi). A new control valve, located in the target return line, will be used to throttle the flow (see Figure 2). This analysis provides the flow conditions (velocities, Reynolds numbers, pressure drops) for each disk and channel, for the following cases:

a) Two main pumps running (normal operation)
b) Broken springs (abnormal)
c) Total flow rates 5 to 150 gpm (parametric study for developing performance curves).

The notes on Figures 4 and 5 (below) correspond to the flow conditions for the normal operating case.

Flow rates from these calculations, used in conjunction with the Dittus-Boelter correlation, provide convective coefficients which are used in turn as input for the calculation of the temperature profiles in the disks.

III. Disk Temperatures and Stresses

We have modeled disks of both one inch thickness and one-half inch thickness using the finite element computer code ANSYS. The HETC/VIM Monte Carlo code provides internal heat generation rates, which for these purposes we take to be at the upper 3σ limit computed for 500 MeV, 20 μA, 3.0 cm fwhm diameter proton beam conditions (the maximum operating case). A curve

FIGURE 4

HYDRAULIC COMPUTER MODEL FOR THE BOOSTER TARGET

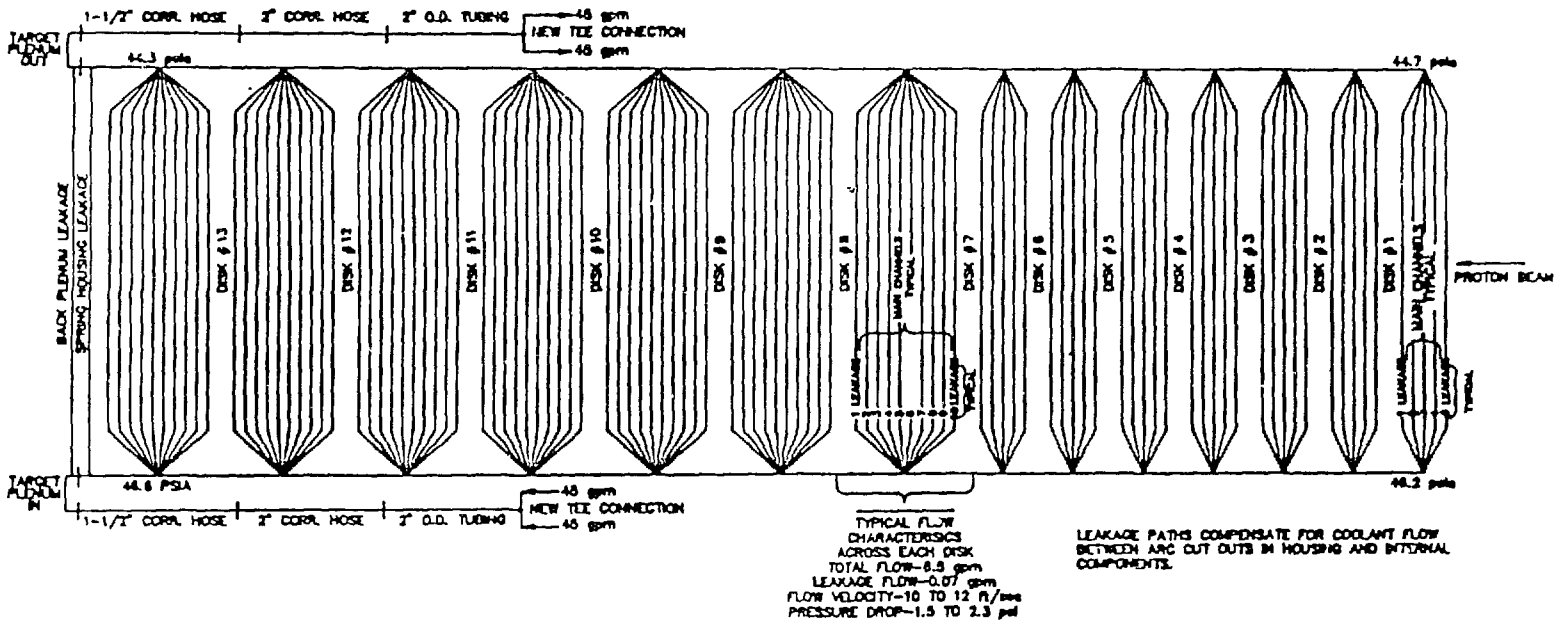

Fig. 4 Hydraulic Model for IPNS Booster Target

fitting routine smoothes the radial power density profile, which we assume has an underlying functional form

$$P(r) = P_o/(1. + ar^2 + br^4),$$

from the Monte Carlo data, binned into four radial bins, and provides data in thirty-eight radial bins for the ANSYS code. We assume the axial power density distribution to be uniform within each one-half inch thick disk, and uniform within each of the two one-half inch regions of each one inch thick disk. The hydraulic analysis provides convective boundary conditions at the disk faces, where we assume for the convective coefficient an area-weighted average over the entire disk face. We assume that the disk circumferences are insulated.

We have calculated the temperatures and stresses in disks #2, #3, #4, #7, #8 and #12 for the maximum operating case. Figure 5 summarizes the results, showing the center temperatures (maximum uranium temperatures) and clad surface centerline temperatures (maximum surface temperature in the flow channels). The highest temperatures both in the uranium (527 °F) and on the surface (248 °F) occur in disk #2; therefore that disk has been used in detailed studies of the off-normal and parametric studies. The hydraulic analysis has determined that the minimum saturation temperature in the flow channels is 267 °F; this provides a heat flux margin of 13% against nucleate surface boiling in the channels. Figure 6 shows the temperature distribution in disk #2. This distribution is the basis for the thermal stress analysis described below.

The thermal analysis for the broken springs case uses the convective coefficients calculated from the hydraulic analysis for that condition. We calculate temperatures for two cases of blocked channels; with the central flow path blocked and with both outer flow paths blocked. Results from these cases indicate that some clad damage may occur under these off-normal conditions, but that no significant safety issues arise.

We have studied the effect of a nonbonded cladding region by calculating temperature distributions for several different sizes of circular insulated areas centered on the face of the disk, and the insulating effect of the spacer by calculating the temperature distribution for an insulated circular region the same width as the spacer strip. Results of these calculations indicate that nonbonds of 1/8 inch diameter and smaller and the 1/8 inch wide spacer strips, have little effect on the temperature distribution in the target disks.

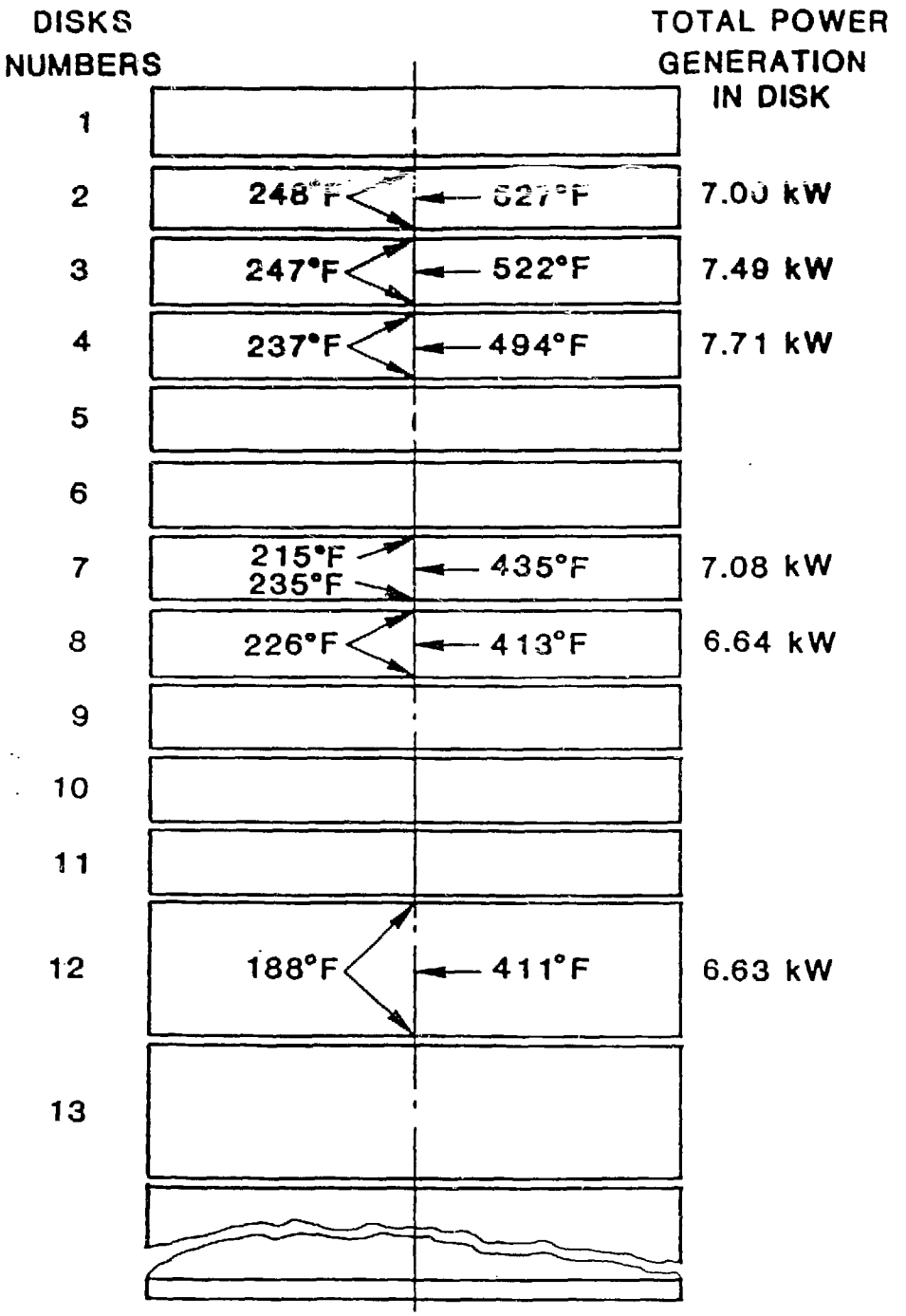

Fig. 5 Maximum Surface and Internal Disk Temperatures at 500 MeV, 20 μA, 3.0 cm fwhm, Operation

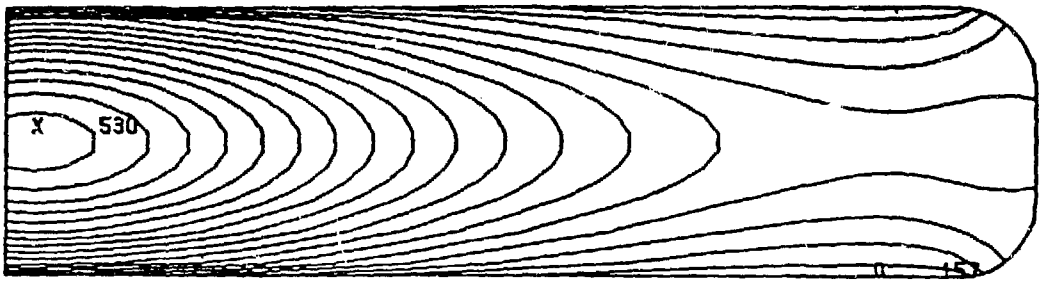

Fig. 6 Temperature Distribution for the #2 Disk at 500 MeV, 20 μA, 3.0 cm fwhm Operation

Disk Thermal Stresses

Using the ANSYS code we calculate the stresses that result from thermal cycling of the disks due to shutdown and startup of the proton beam. The fatigue life of the Zircaloy cladding places limits on the number of thermal cycles and hence the usable target lifetime. Detailed parametric studies show that under worst case coolant flow conditions (90. gpm, 120°F) and with maximum proton beam power the highest clad stresses occur in disk #2. For this one-half inch thick disk, the stress intensity (SI) in the clad at the center of the disk face varies from 0 to 43000. psi; the maximum alternating stress is one-half this value, 21500. psi. On the basis of experience to date, we expect about ten thermal stress cycles per day.

The maximum alternating stress in the cladding occurs on the outer surface of the clad and in the center of the disk, so that cracks are expected to initiate on the outside surface. It is encouraging to note that the maximum alternating stress at the interface between the clad and the uranium is only 13600 psi. Figure 7 shows the contours of the stress intensity in disk #2.

The fatigue curve for irradiated Zircaloy-2,[4] valid between room temperature and 600 °F (see Figure 8), indicates that for an alternating stress of 21500. psi, failure from fatigue occurs after approximately 100,000 cycles. Thus we can expect the fatigue-limited lifetime to be 10,000 operating days, or about 27 years of continuous operation. The data indicate that all samples fail at higher stresses and numbers of cycles than those corresponding to our conditions, so that we have a considerable safety margin in this respect.

IV. Decay Heat Analysis

Spallation product and especially fission product decay heat in the Booster target is sufficiently higher than in the present depleted uranium target to require special analytical attention and the inclusion of a decay heat removal system. We have used the thermal transient computer code THTB for this analysis, assuming that the shutdown decay heat source follows the Wigner-Way description of the decay of fission products but assuming the operating target power is the total due to fission and spallation and proton beam energy loss. Calculations for disks at uniform temperature show that stresses in the disks and cladding remain at safe levels as long as the temperature is below 600°F; we use this criterion to guarantee no damage to the disks in thermal excursions.

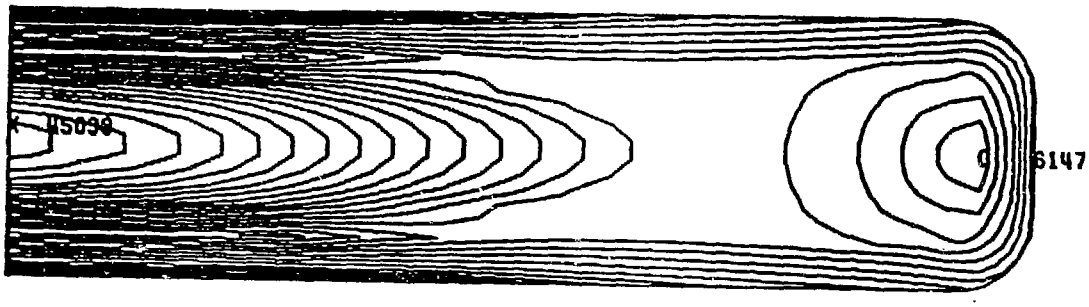

Fig. 7 Stress Intensity Distribution for the #2 Disk at 500 MeV, 20 μA 3.0 cm fwhm Operation

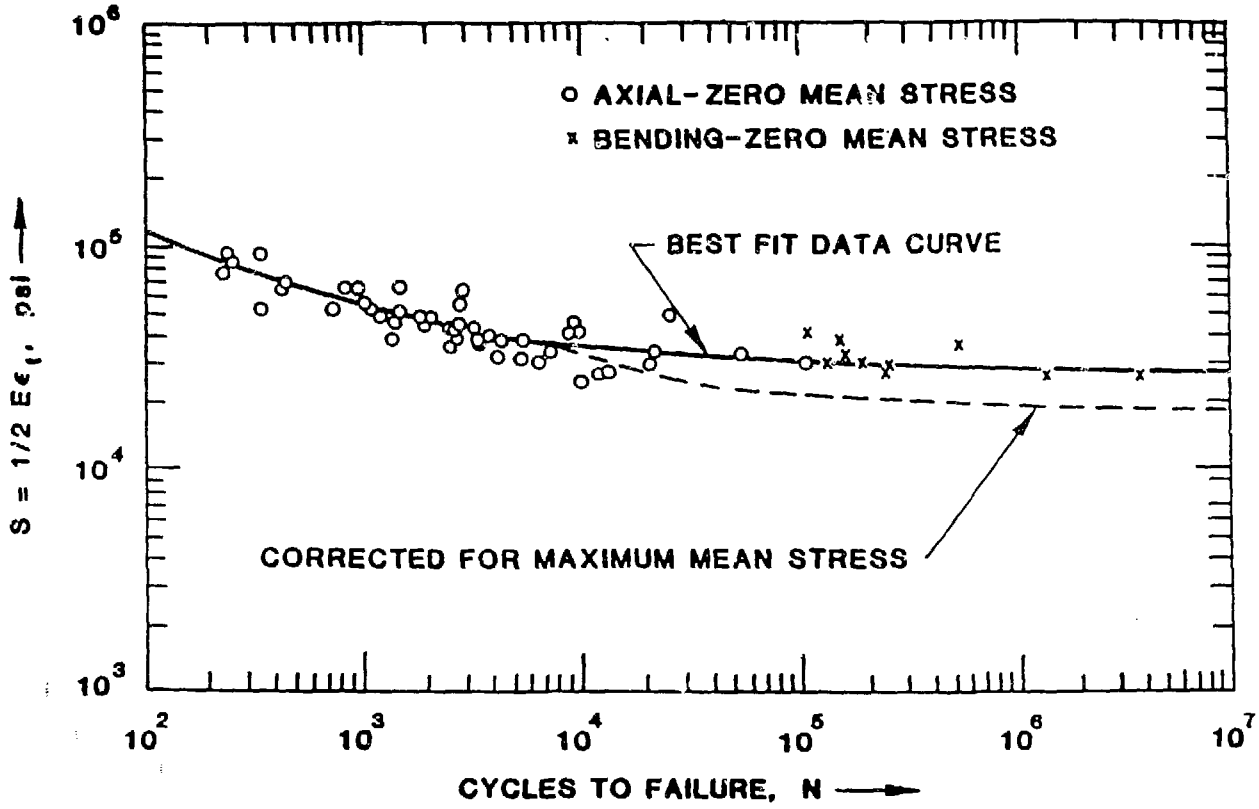

Fig. 8 Irradiated (1.5×10^{21} to 5.5×10^{21} nvt) Zircaloy Fatigue Data Curve - Room Temperature to 600F

We have developed two models to study conditions under normal and off-normal conditions. Figure 9 shows both the 1/4-round and the 1/2-round models. We have studied the following cases:

a) Coolant flow requirements under beam shutdown conditions (used to decide the size of decay heat removal pumps) - normal.
   Result: 2 gpm flow is required to prevent damage to target disks.

b) Decay time required before cooling can be stopped (used to determine requirements for safe removal and storage of the irradiated target) - normal.
   Result: 45 days of cooling are required to prevent damage to target disks.

c) Stoppage of primary flow with proton beam off (used to determine the length of time before cooling must be provided) - off normal.
   Result: A minimum of 11 hours are available until damage occurs to the target disks.

d) Total loss of coolant (used to determine whether autocatalytic ignition of Zircaloy cladding occurs, and that the temperatures remain below the melting temperature of all materials)- off normal.
   Result: Figure 10 shows the temperatures of various materials as a function of time, assuming infinite prior operation. Some oxidation but no autocatalytic ignition of cladding occurs; no materials melt.

e) Stoppage of secondary flow through heat exchanger (used to determine the length of time before remedial measures must be taken) - off normal.
   Result: After 22 hours, the primary coolant temperature reaches 180 °F, at which temperature cavitation begins in the primary pumps.

V. Radiation and Thermal Cycling Growth

During operation, the Booster target disks will undergo anisotropic dimensional changes that could limit the target lifetime by opening bypass coolant flow paths, closing coolant flow paths, straining the target vessel or cracking cladding. Irradiation-induced growth and thermal cycling growth depend on the grain size and the degree of preferred orientation (texture) of the uranium; we are currently quantifying these characteristics of the material by neutron diffraction methods. Figure 11 compares the neutron diffraction patterns of randomly-oriented uranium and the as-cast Booster target material, from a depleted uranium test casting. Measurements were made at the IPNS Special Environment Powder Diffractometer. Further,

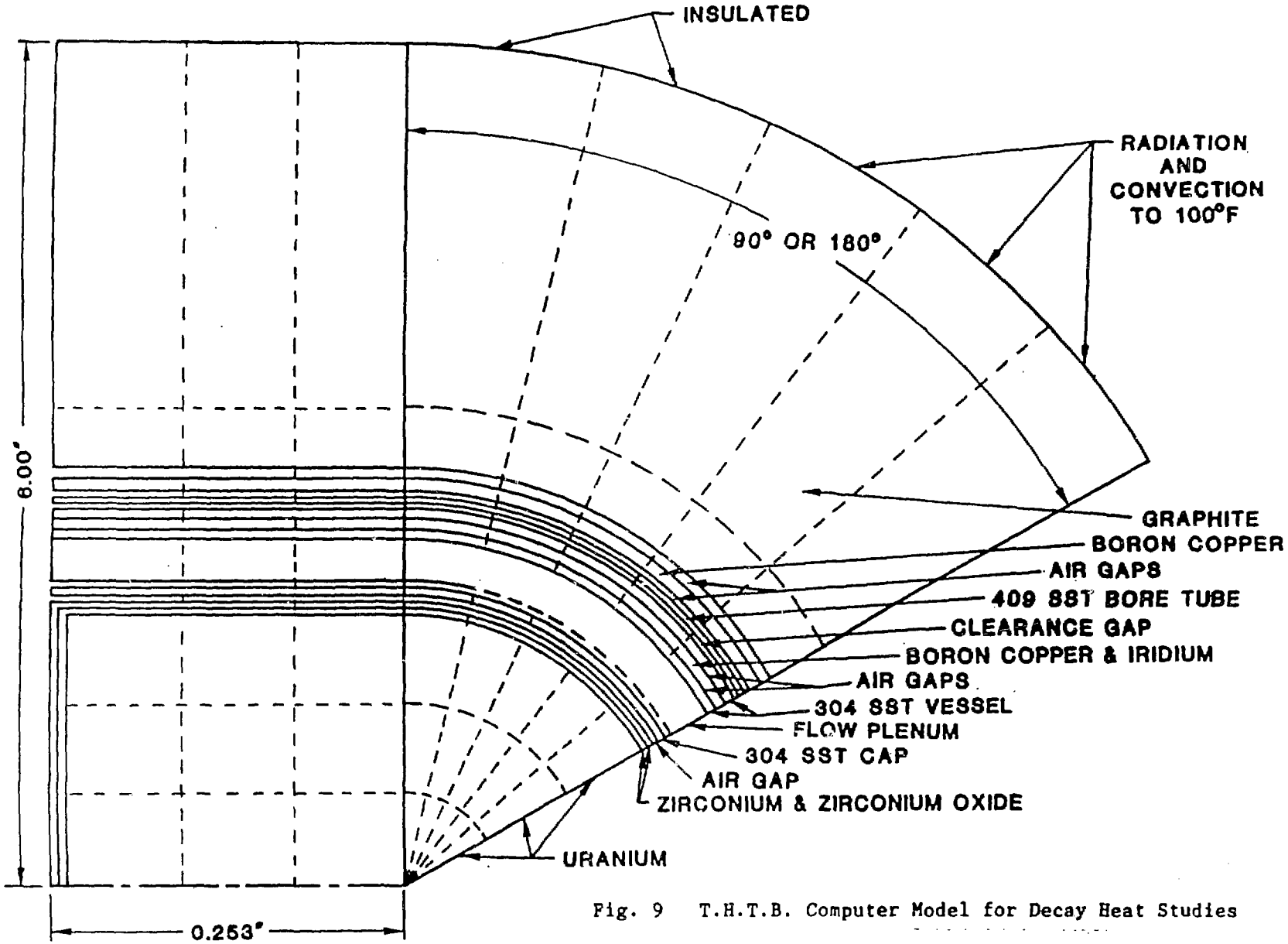

Fig. 9 T.H.T.B. Computer Model for Decay Heat Studies

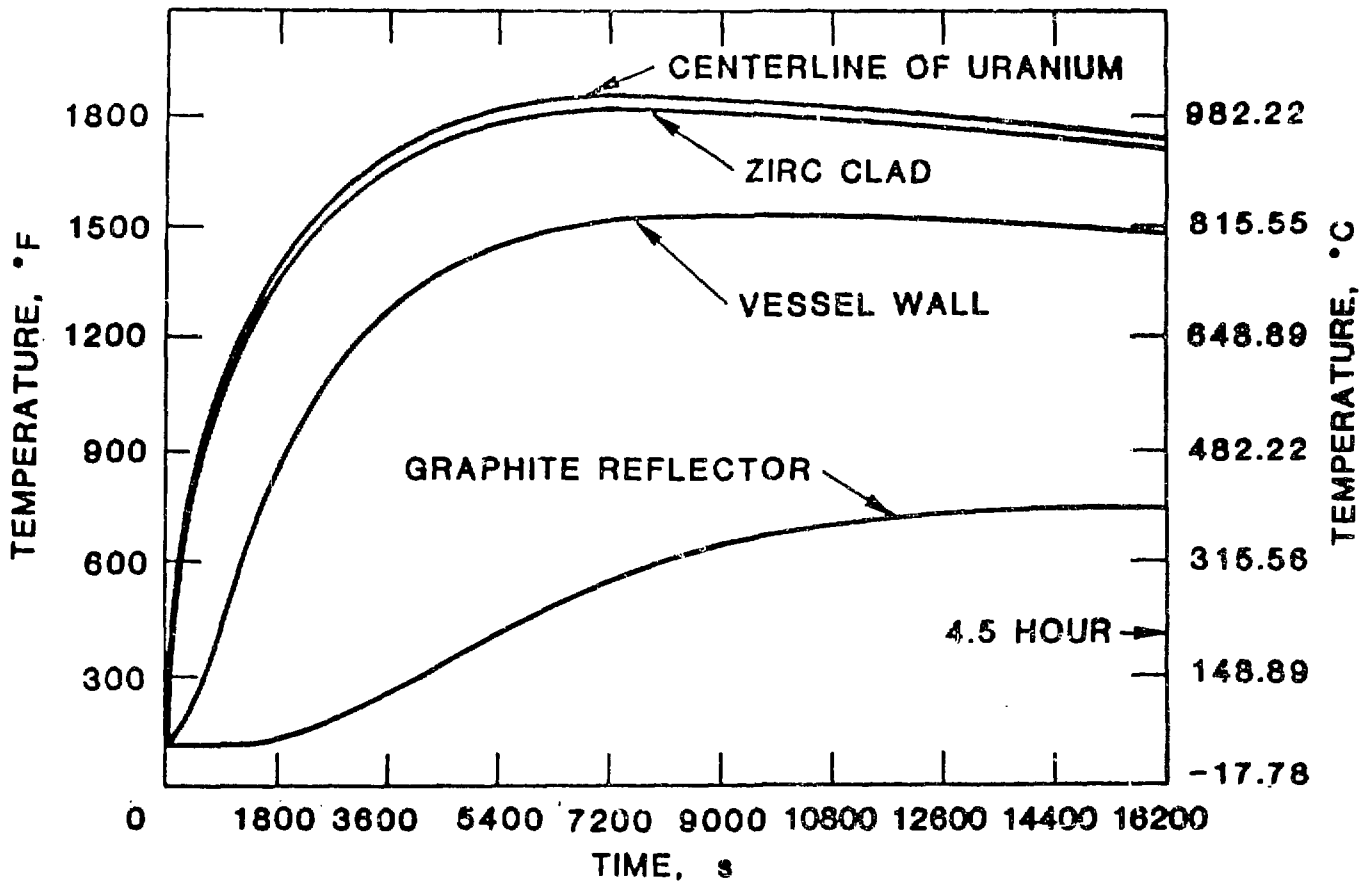

Fig. 10 Thermal Transient for the Loss of Coolant with Decay Heat and Zirconium Oxidation Case

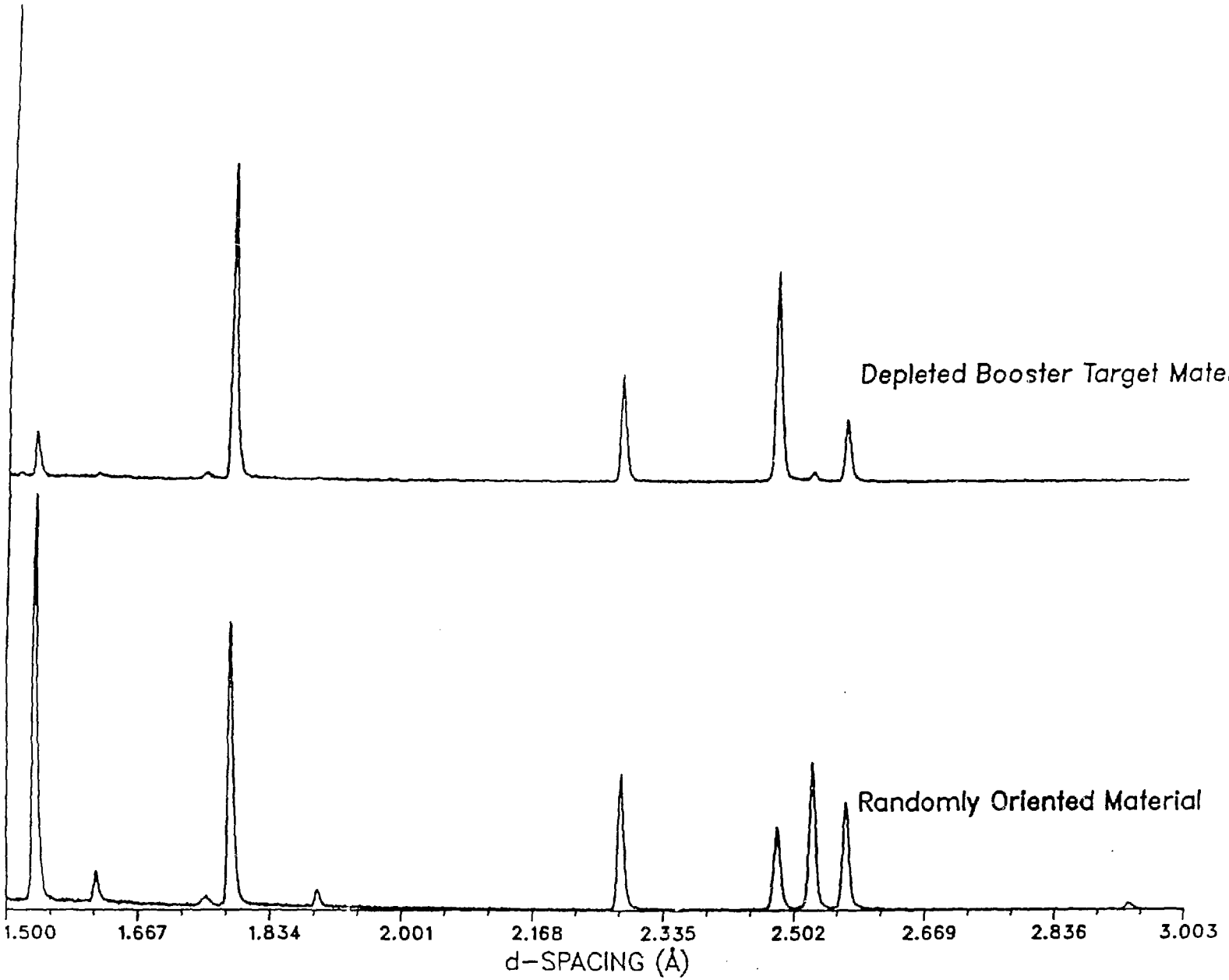

Fig. 11 Neutron powder diffraction patterns of randomly-oriented depleted uranium and of as-cast (depleted) Booster target material.

quantitative texture measurements are being made at the powder diffractometer and the single crystal diffractometer at the Missouri University Research Reactor. Preliminary texture measurements and analyses have shown that irradiated target disks will exhibit a net radial shrinkage and a net axial growth exceeding the volumetric swelling due to solid fission products, gaseous fission products and cavitation.

The volumetric swelling rate is $\Delta V/V = 5.2 \pm 0.06$ %/at% burnup [5,6]; since this swelling is isotropic, the relative length change is $\Delta l/l = 1.7 \pm 0.02$ %/at% burnup. Anisotropic growth takes place without net volume change. For nominal operating conditions, 16 μA, 450 MeV. 3. cm fwhm proton beam diameter, and 26 weeks per year operation, the maximum radially-averaged burnup rate is 0.063 at%/yr, and the maximum central burnup rate is 0.08[illegible] at%/yr. The target can accommodate at most 2 % radial shrinkage of the uranium before bypass flows become troublesome, and at most 9 % axial growth before the springs become fully compressed. If anisotropic growth rates were known and included in the calculations of the dimensional changes, the time to exceed these limits can be estimated. For example, if the anisotropic growth rate is $\Delta l/l = 54$%/at.% burnup (current estimate derived from texture measurements[7] on as-cast, HIP treated material, for unalloyed, unrestrained uranium) and the radial shrinkage rate is 27%/at.% burnup, then the lifetime of the target would be about 1.3 years, limited by radial shrinkage. Axial growth limits would be exceeded after 2.1 years. We are considering β-phase heat treatment to reduce the texture of the material and mechanical means to accommodate the growth, meanwhile assessing the accuracy of these predictions. Recall that the estimate of lifetime considering clad fatigue failure for continuous operation and more severe circumstances is about 27 years.

The average target burnup, conservatively assuming five years at the expected operating conditions and duty cycle is 0.225 at% and the concomitant peak burnup is 0.75 at%. The effects on target structural materials other than uranium, due to nuclear radiation associated with these burnup figures, are negligible except in the case of the cladding, which we have taken into account by use of data for irradiated Zircaloy in estimating clad fatigue life.

VI. Disk Fabrication

Assembly Process Description

Oak Ridge Y-12 plant, with technical support of ANL, is fabricating the clad, enriched uranium disks. Casting, machining, bonding, and inspection

procedures are adaptations of the methods developed at ANL for producing the depleted uranium target. Figure 1 above shows the target disk and vessel design. Electron beam welds seal the split cladding cans on the disk circumference. A high temperature and pressure HIP bonding operation creates a diffusion bond between the cladding and the uranium core. Final machining reduces the initially .060 inch thick cladding to .040 inches on the circumference and .020 inches on the faces.

Process Qualification

This phase of the work employed depleted uranium alloy material to establish proven processing, manufacturing and inspection procedures. Y-12 has produced, assembled, bonded, and tested four qualification disks, two of 1/2 inch thickness and two of one-inch thickness. Argonne provided the machined cladding cans. Due to criticality considerations, we substituted the Y-12 process of vacuum induction casting into a rectangular slab mold, for the ANL procedure of consumable arc casting. To provide the required high purity atmosphere during bonding, we installed at Y-12 an upgraded, small HIP bonding unit from ANL. A single cycle does not always produce complete bonds in the corners of the disks. This is due to the mismatch of the volume contraction and stiffness of uranium and zircaloy, which stresses the interface upon cooldown, leaving the clad in compression. Little is known about the strength of the bond, but the extrusion constant is a good measure of the stiffness of the materials: 6000 psi and 16,500 psi for uranium and zircaloy-2 respectively at 820°C and 30,000 psi and 50,000 psi at 650°C. The difference aggravates the problem of clad-core separation during cooldown. A second cycle shows a good probability of bonding disks which have flaws after the first cycle.

We have examined three qualification disks nondestructively and destructively to characterize the materials and verify the adequacy of the design. Measurements included determining chemical additive content, uranium grain size and texture, clad weld penetration, clad-core bond quality and machined final clad thickness. Final review has determined that the established procedures are capable of providing acceptable target disks.

Disk Production

Clad Can Fabrication. ANL has fabricated the Zircaloy-2 cladding cans from a 4-1/2 inch diameter annealed forging. The nominal 4 inch diameter, 1/2 or one inch deep, .060 inch thick cans have closely-held dimensions

chosen to allow convenient assembly and tight fitup at bonding temperature. Drumhead bowing and weld face warpage are persistent problems that we have overcome by reducing the machining cuts to small, closely-controlled steps and using special hold down fixtures, pads and clamps. The inner surfaces of the cans must be free of foreign matter to promote diffusion bonding. Adjustment of machining speed, feed rate and cutting lubricants has produced surfaces of the needed quality.

Thermowell Tube Fabrication. ANL has also produced the thermowell tubes, machined from 1/2" diameter round stock, 2-3/8" long, drilled to provide a hole of final size. Special precautions prevent hole arching. After drilling, the outer diameter is machined concentric with the bore. A gas tungsten arc weld bead seals the end of each finished tube; x-ray inspection verifies the quality of the weld.

Uranium Core Casting. Enriched uranium feed material is melted by a vacuum induction technique in a graphite-coated crucible. Elemental alloying additives, nominally 350 ppm Si, 250 ppm Fe, and 450 ppm C, combine in the melt to produce an composition resistant to thermal cycling growth and irradiation swelling. The melt is held at 1325 °C for 15 minutes, poured into a graphite book mold coated with a mold wash of ZrO_2-$ZrSiO_2$ and air cooled. The size of the castings for one-inch thick disks is 1.3" x 4.5" x10"; for 1/2" thick disks, 3/4" x 9" x 9". Standard machining practices produce finished cores. Carbide drills introduce holes for the thermowells; overcoming problems of stuck drills and hole runout requires trial and error experience. Core blanks provide samples for chemical analysis and metallography. As-cast uranium grains are approximately of ASTM size 2, with prominent subgraining as shown in Fig. 12.

Disk Assembly and Bonding. Cleaning inspected disk components before assembly and welding is essential. Wire brush cleaning removes surface oxidation from the inside surfaces of the Zircaloy cans. Manual cleaning with a Skotch-Brite pad, followed by a pickling dip in nitric acid, a rinse in a bath of isopropyl alcohol and wire brushing, prepares the uranium adequately. Visual inspection of the uranium surface shows whether or not the surface oxide, as indicated by a mottled, darkened appearance, has been removed. Proper cleaning of the uranium is critical for success in diffusion bonding.

Metal handling tools insert the uranium core into the cladding cans in a dry box atmosphere; a radial 0.005" core-clad gap and 0.003"-0.008" axial gap optimize the fitup during assembly. Next the assembly is placed in the

Figure 12. Typical Cast Uranium Grain Size Distribution Magnification (approximately x100) is such that the base of the figure represents 1.3 mm. ANL Neg. MS-85-0718-2

electron beam welding chamber and evacuated. The weld seals the can halves on their circumference as the assembly is rotated. Selected and qualified welding parameters effect the proper penetration, which extends 30-70% into the clad wall. Excessive penetration causes uranium alloying in the weld, and catastrophic cracking. The clad separation beneath the weld joint heals completely during the HIP bonding process. Electron beam welds also seal the thermowell tubes to the cans. Welding must be done in a short time after cleaning and assembling the components, meantime they must be stored in inert containers.

A Hot Isostatic Pressure bonding process produces a metal-to-metal bond between the cladding and the uranium of the sealed disk assemblies. A bed of Zirconium chips accompanies the disks in the bonding unit, as a getter of impurities. Purge cycles of evacuation and introduction of high purity argon gas and the use of the getter chips prevent heavy oxidation of the cladding, which makes it very stiff and seems to lead to debonding during cooldown. Following a one-hour heatup to 840. °C and pressurization to 25,000. psi, the temperature and pressure remain at the maximum for three hours; a controlled, slow cooldown at 1. °C/min follows until the temperature reaches 200. °C. The expected superficial oxidation of the cladding can be removed by emery paper. Figure 13 shows a typical clad-core bond zone.

Final machining produces close tolerances on disk thickness and diameter. HIP bonding produces some undulation of the disk surfaces, so that precise disk surface maps have to be made before alignment in the lathe. Frequent measurements during machining enable the clad face thickness to be held in the range 0.017/0.025".

Inspection. Chemical analysis of the cast uranium core samples give the Si, Fe, and C additive content as well as the content of other metallic impurities. These results along with examinations of grain structure in metallographic sections and crystallographic texture in diffraction samples, provide for the assessment of uranium swelling.

Ultrasonic tests check the entire disk surface, including the rounded corners, for completeness of bonding, and can detect nonbonded areas down to a diameter of 1/16". Y-12 and ANL test methods compare successfully. Calculations indicate the thickness of cladding after final machining, although this approach presents some difficulties. We spot-check the clad thickness with a portable ultrasonic unit calibrated against standards of known thickness.

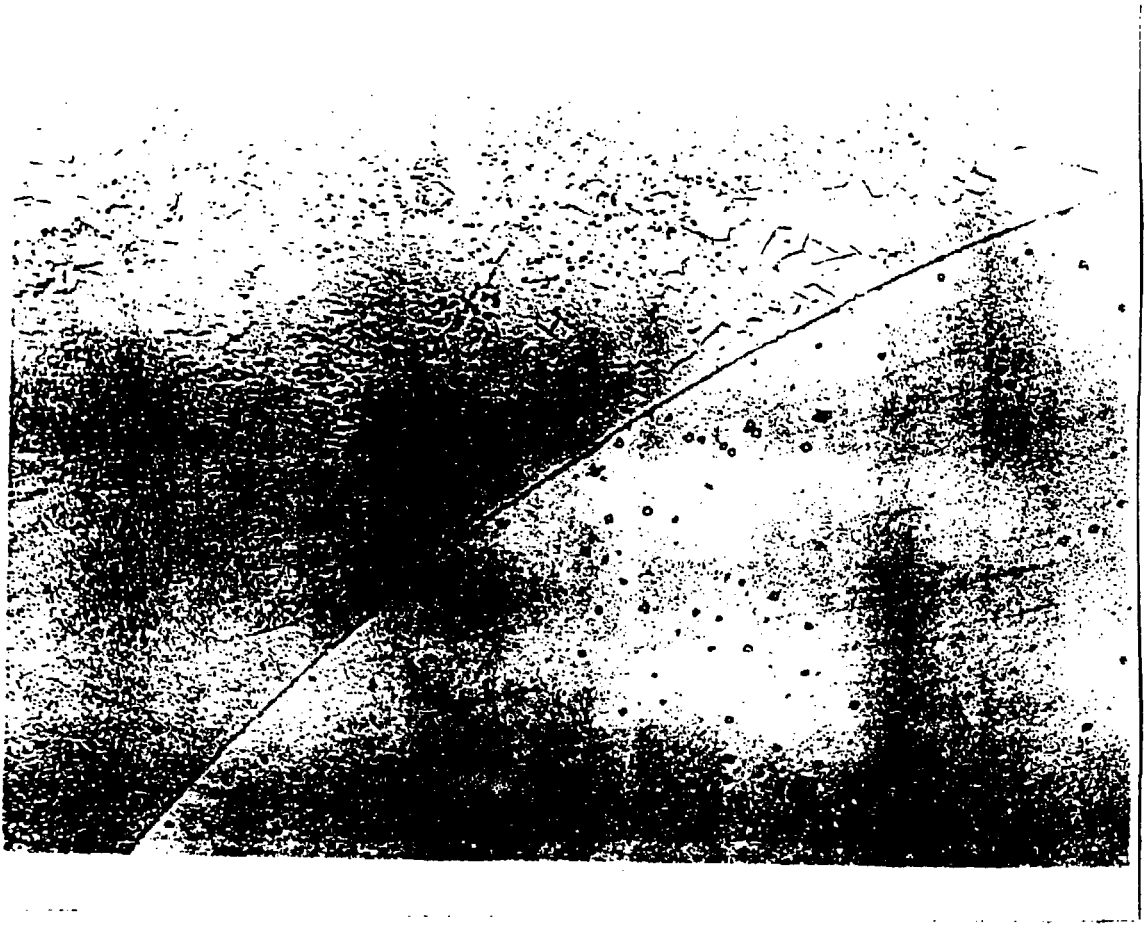

Fig. 13 | **Typical Clad-Core Bond Interface After HIP Bonding at 840°C for Three Hours**

Other inspections which take place throughout processing and prior to shipment include mass spectrometer leak testing, visual inspection, weighing, measurement of thermowell dimensions and checks for surface uranium contamination.

VII. Radiological Hazards

We expect the highest long-term operating conditions to correspond to 16. μA, 450. MeV proton beam current with a beam size between 3. and 4. cm fwhm diameter. These conditions will produce 56. kW total thermal power (49.2 kW fission, 6.8 kW spallation), although we have assumed higher values for purposes of conservative design. Because of this relatively low power and because we expect to operate only about half the time, the radionuclide inventory is not so large as to constitute a significant radiological threat to the public. We have demonstrated this through an analysis based on the most probable mechanism of release of radionuclides to the coolant water, that is a crack in the cladding in the most highly stresed target disk. The analysis further conservatively assumes (1) five years' continuous operation at 18. μA, 500. MeV (total power 74.9 kW), (2) 30 days' continuous operation after a clad crack 1. mm wide develops across the face of a disk (normally, this would be detected in no more than four hours in the course of regular monitoring of gas samples), and (3) a breach of the target cooling system which releases all the cooling water to the atmosphere. We have assessed the consequences both of the water being filtered through the IPNS effluent control system and when it is released unfiltered (as a result of a tornado or earthquake, for example).

The computer code ORIGEN has calculated the fission product buildup, ORIHET computed the spallation product buildup, and DOSER determined the hazard of the release to a receptor at the ANL site boundary[8]. The basis for the case of unfiltered release is that 100% of the noble gases, 50% of the halogens and 0.1% of the solids are released; for the unfiltered case the fractions are 100% of the noble gases, 50% of the halogens and 10% of the solids. Both analyses assume a wind speed of 1. m/sec and Class F wind stability conditions. Table 2 shows the results, expressed as a fraction of the 10CFR100[9] guideline values.

Table 2
Clad Breach Dose Consequences

ORGAN	10CFR100 GUIDELINE DOSE, rem	DOSE IN FILTERED CASE, %	DOSE IN UNFILTERED CASE, %
Bone	150.	1.8×10^{-4}	0.016
Lung	75.	2.0×10^{-3}	0.19
Thyroid	300.	5.4×10^{-3}	5.4×10^{-3}
Whole Body	25.	4.7×10^{-4}	9.6×10^{-3}

The highest dose is 0.19% (0.14 rem) of the lung guideline dose which is not a significant hazard.

The increased radiation from the Booster target (about ten times that of the present target for the same operating conditions) while in operation or when shut down necessitates only minor changes in the main shield, and some changes in the target handling procedure. The increased radiation during operation will not cause any increase in groundwater activation above that of the present target.[10]

VIII. Neutronics and Power Densities

The complexity of the Booster target configuration suggests the application of a Monte Carlo code to the neutronic analysis, rather than a mesh-based analysis. We used Argonne's neutral particle radiation transport code VIM.[11] Since the Booster assembly is very small, it is intimately neutronically coupled to its environment. The spectrum in the target is very hard, but the surrounding media are mostly thermalizing, and contain large voids and localized strong absorbers, so there is no reliable way to postulate a fundamental mode neutron distribution to be used for multigroup cross section generation. VIM's use of combinatorial geometry and of detailed, composition- and spectrum- independent, continuous-energy cross sections and scattering distributions eliminates these problems altogether. Accordingly, we have used VIM for all neutronic design calculations, except for estimation of the prompt neutron generation time, for which we used KENO.

Having chosen from survey calculations the operating $k_{eff} = .80$ as providing approximately the desired design features, we have determined the required enrichment to be 77.5% from a series of eigenvalue calculations

performed for various values of enrichment. Subcriticality is assessed (and assured) in a variety of cases in which the Booster is completely surrounded by different materials which either are encountered during fabrication, transport and installation, or might be encountered in off-design circumstances. The ^{10}B decoupler layer in the vessel wall is assumed to remain in place for the purpose of these calculations. Table 3 shows the results. Since the Booster must pass through the beryllium outer reflector during insertion and removal, we have modeled these two situations in more realistic detail. These cases are conservative because the absorbing media associated with the moderator-reflector assembly and the iron constituting the main shield are represented as beryllium. As shown in Table 3, k_{eff} = 0.92 in both these cases, which differ in that in the removal case, we have accounted for the (estimated separately for 5 years operation at 20 μA, 500 MeV) 2.5% burnup of the ^{10}B decoupler.

Table 3

Booster Eigenvalues in Various Configurations

DESCRIPTION	k_{eff}
Bare	0.6660 ± 0.0034
Embedded in CH_4	0.7337 ± 0.0062
Embedded in H_2O	0.7523 ± 0.0046
Embedded in concrete	0.8119 ± 0.0060
Embedded in iron	0.8346 ± 0.0038
Embedded in natural uranium	0.8860 ± 0.0049
Embedded in graphite	0.8900 ± 0.0064
Embedded in beryllium	0.9362 ± 0.0051
During insertion	0.9200 ± 0.0035
During removal	0.9179 ± 0.0069

We calculate the power densities required for thermal-hydraulic, activation, and other analyses, using four radial bins in each disk. This is done in two steps; first using the High Energy Transport Code HETC[12] we simulate the transport and the heat generation of the incident protons, high energy fission and spallation processes. VIM then picks up the calculation for neutrons using the source site tape written by HETC, which contains the

spatial coordinates, energies and directions of all the neutrons born or downscattered below 15 MeV. About 30 additional generations (99.999%) of all neutrons born in subcritical multiplication are included in the VIM simulation. The resulting heat generation rates are the sum of the HETC estimates and the VIM fission rates, assuming 190. MeV is deposited at the fission site. Figure 14a shows the power density distribution. For these calculations we take the proton beam to have a full width at half maximum diameter of 3. cm, slightly larger than the radial mesh width of 1.27 cm. This radial peaking is evident when comparing the dominance of the fundamental mode axial profile in the outermost annulus to the front-peaked centerline profile. The rapid falloff of the power density in the downstream end of the target is due to the finite range of the protons. Figure 14b shows the two computational (and physical) components of the power density in the central zone: high energy interactions (HETC) and lower energy fissions (VIM). The fission rate density is peaked in the front due to the high density of source sites produced by high energy interactions (HETC), and its subsequent relaxation to the fundamental mode. We have found in a separate study that, in addition to producing more primary neutrons, higher energy protons excite the fundamental mode more efficiently than lower energy protons, and thus produce multiplied neutrons more than in proportion to the primary spallation yield.

The efficacy of the Booster has been demonstrated by calculating the neutron flux (track length) in a 1.4 cm-thick slab at the surface of a room temperature polyethylene moderator in position "C", on the side facing the neutron beam tube, and comparing the Booster with the present, depleted uranium target. Both calculations use the same HETC-generated primary neutron source, and employed modest splitting and Russian Roulette techniques to improve the efficiency of the calculation. Figure 15 shows that the shapes of the spectra are nearly identical, and larger in the Booster case than in the depleted target case by a factor of about 3.0.

We have used the Monte Carlo code KENO[13] for three purposes: (1) in safety-related assessments of the multiplication factor, for aggregations of free target disks and the assembled target in various media; (2) to determine the prompt-neutron generation time l_p and thus provide an estimate of the prompt pulse width $\tau \lesssim l_p/(1 - k_{eff})$); and (3) to perform check calculations of k_{eff} to compare with VIM results for several identical cases. The calculations show that subcriticality is guaranteed under all conditions of assembly, operation, and disposal. KENO is a criticality safety code,

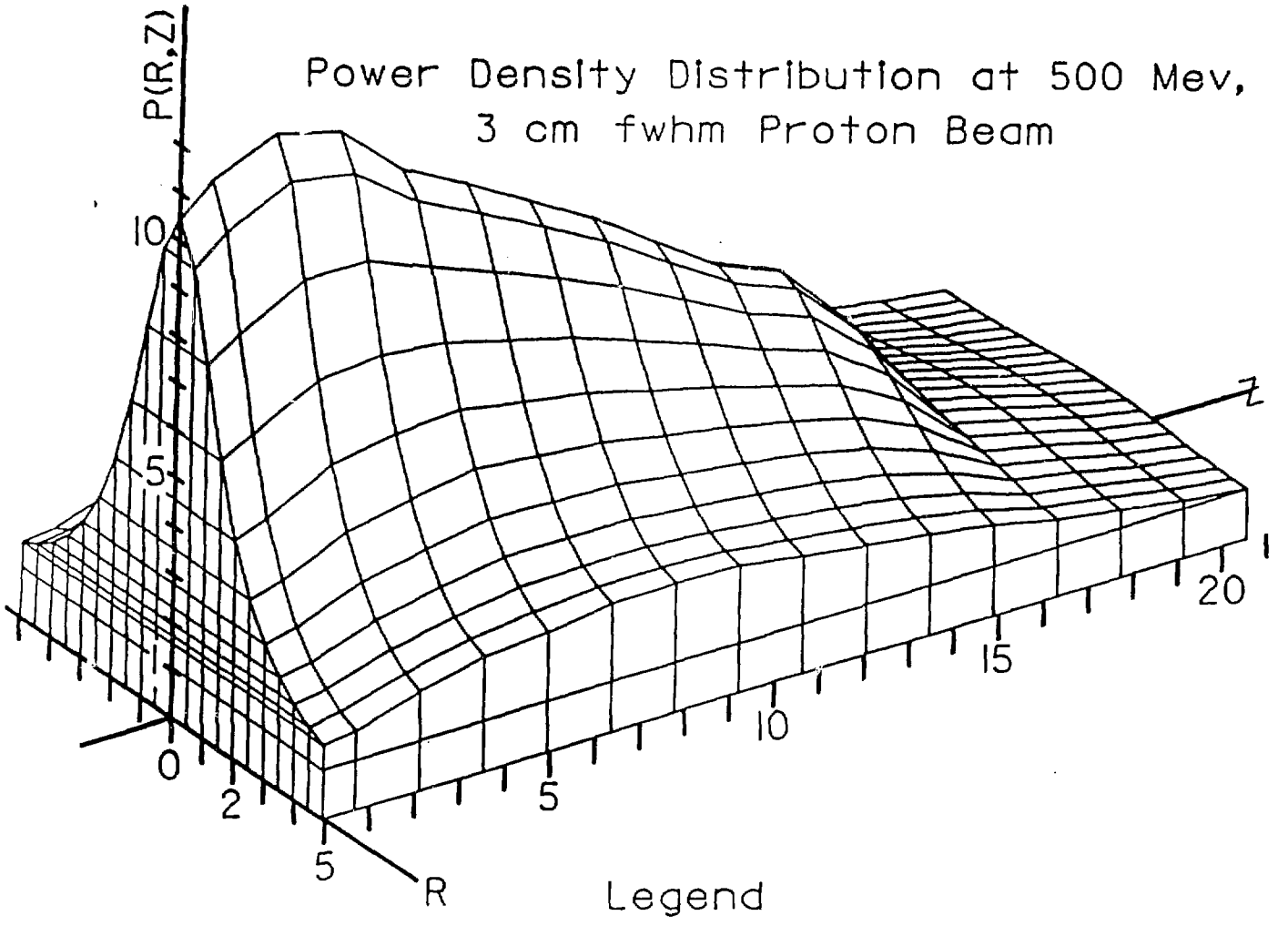

Fig. 14a The Power Density Distribution in the Booster Target

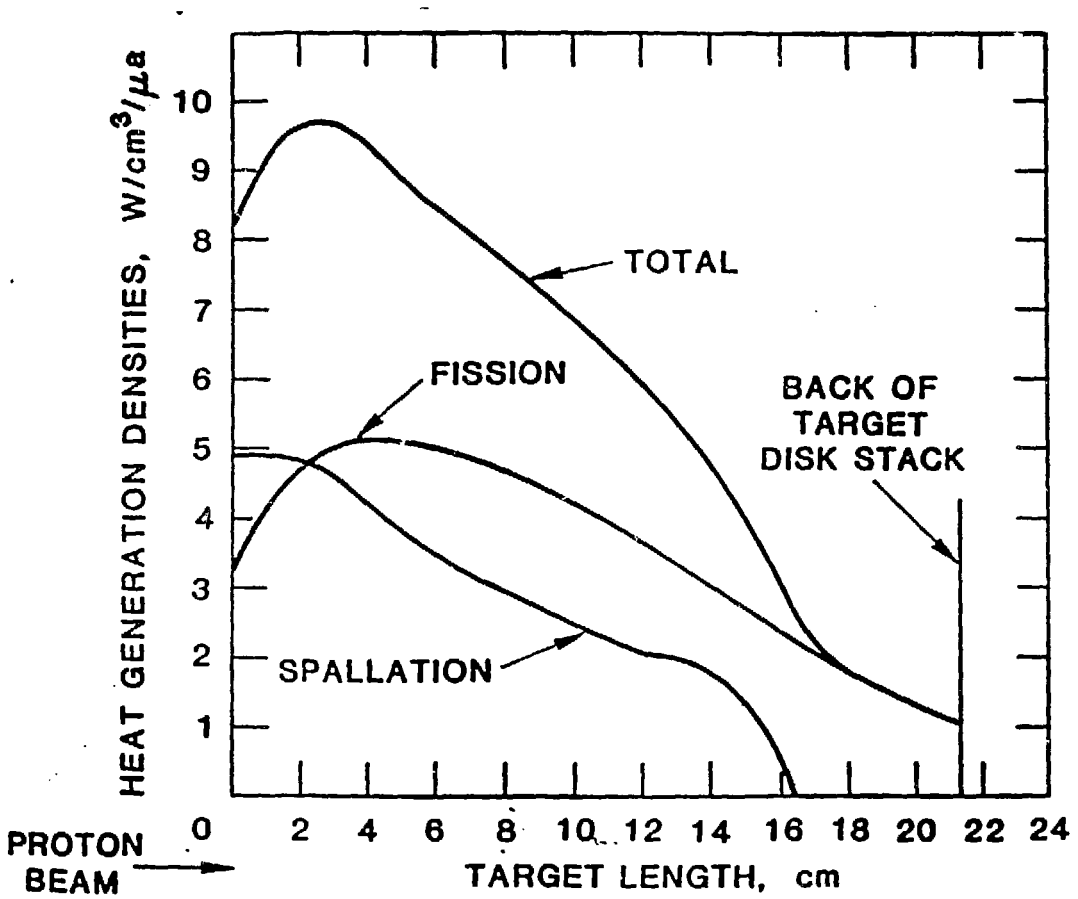

Fig. 14b Axial Centerline Profiles of the Internal Heat Generation in the Target Disks Due to Fission and Spallation and the Total

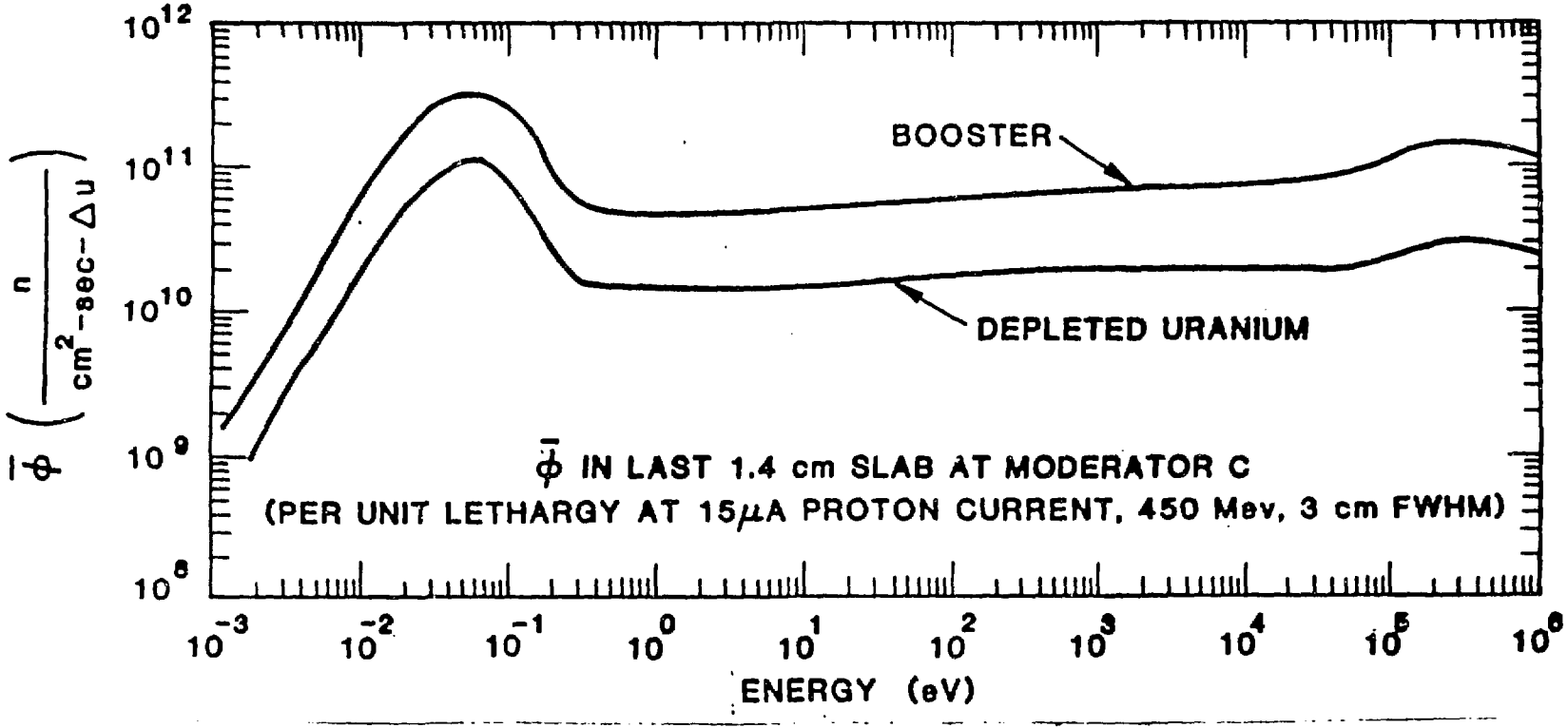

Fig. 15 Average Moderator Neutron Scalar Flux Spectra for the Depleted Uranium and the Booster Targets

which is known to be more conservative than VIM; as expected, the KENO k_{eff} values are always higher (Δk_{eff} = 0.01 - 0.03) than those from VIM. The prompt generation time is found to be 68. nanosec, and the Booster response time accordingly estimated to be 340. nanosec. This does not affect moderated neutron pulse widths significantly for energies below about 6. eV in a typical moderator. If the inner reflector were beryllium rather than graphite, and the coolant were D_2O rather than H_2O (design options that we have recognized but not employed for economic reasons) the Booster response time would be 43. nanosec., while the estimated pulse width would be 215 nanosec.

IX. Safeguards and Security

Because of its significant content of special nuclear material (^{235}U) and (eventually) of radioactive materials, the fabrication, operation and disposal phases of the Booster target are subject to safeguards and security regulations and controls. The design and operation of the target and supporting systems fully accommodate these regulations, and attention to them has been a substantial part of the design and planning activity. This aspect of the work has been facilitated by our continuous and early consideration of these issues.

X. Summary

We have described the design and evaluation of an enriched uranium booster target for IPNS. The new target will be installed in the near future, without extensive modification of the facility, and meets all the criteria for safe operation. The Booster will increase the intensities of the neutron beams, and therefore the effectiveness of IPNS by a factor of three.

Acknowledgement

We express our gratitude to M. H. Mueller, J. W. Richardson, Jr. (Argonne), D. G. Reichel, F. K. Ross and W. B. Yelon (Univ. of Missouri) for their excellent work on the neutron diffraction characterization of uranium. We thank T. Weincek and R. F. Domagala for development and production of the ^{10}B-Cu composite decoupler material.

REFERENCES

1. A. W. Schulke for the IPNS Enriched Uranium Booster Target Design Team, "IPNS Enriched Uranium Booster Target", ICANS VIII, Proceedings of the Eighth Meeting of the International Collaboration on Advanced Neutron Sources, Rutherford-Appleton Laboratory, July, 1985, Rutherford-Appleton Laboratory Report RAL-85-110, Volume I, 231, (1985).

2. D. J. Erickson, unpublished information, 1984.

3. "Flow of Fluids Through Valves, Fittings and Pipes" Technical Paper 409, Crane Company, 1942.

4. W. J. O'Donnell and B. F. Langer, "Fatigue Design Basis for Zircaloy Components", Nucl Sci & Eng 20, 112,(1964).

5. M. C. Billone personal communication to B. S. Brown.

6. B. A. Loomis personal communication to B. S. Brown.

7. M. H. Mueller and J. W. Richardson, personal communication.

8. D. R. Henley personal communication to A. E. Knox.

9. "Part 100--Reactor Site Criteria", U. S. Code of Federal Regulations, Chapter 10, Nuclear Regulatory Commission.

10. M. M. Barbier, unpublished information, 1984.

11. R. N. Blomquist, "VIM, A Continuous Energy and Photon Transport Code", Advances in Reactor Computations, Proceedings of a Topical Meeting, Salt Lake City, 28-31 March, 1983.

12. R. C. Chandler and T. W. Armstrong, "Operating Instructions for the High-Energy Nucleon-Meson Transport Code HETC", Oak Ridge National Laboratory report ORNL-TM-36607 (1972).

13. L. M. Petrie and N. M. Cross, "KENO IV--An Improved Monte Carlo Criticality Program", Oak Ridge National Laboratory report ORNL-4938 (1975).

FIGURE CAPTIONS

Fig. 1 Booster Target Installed in Moderator/Reflector Assembly

Fig. 2 Cross Section Elevation Through IPNS Facility

Fig. 3 Hydraulic Performance Curves for the Two Cooling Systems Operating in Parallel

Fig. 4 Hydraulic Model for IPNS Booster Target

Fig. 5 Maximum Surface and Internal Disk Temperatures at 500 MeV, 20 μA, 3.0 cm fwhm, Operation

Fig. 6 Temperature Distribution for the #2 Disk at 500 MeV, 20 μA, 3.0 cm fwhm Operation

Fig. 7 Stress Intensity Distribution for the #2 Disk at 500 MeV, 20 μA 3.0 cm fwhm Operation

Fig. 8 Irradiated (1.5×10^{21} to 5.5×10^{21} nvt) Zircaloy Fatigue Data Curve - Room Temperature to 600F. Data from reference 8.

Fig. 9 T.H.T.B. Computer Model for Decay Heat Studies

Fig. 10 Thermal Transient for the Loss of Coolant with Decay Heat and Zirconium Oxidation Case

Fig. 11 Neutron powder diffraction patterns of randomly-oriented depleted uranium and of as-cast (depleted) Booster target material.

Fig. 12 Typical Cast Uranium Grain Size Distribution. Magnification (approximately x100) is such that the base of the figure represents 1.3 mm. ANL Neg. MS-85-0718-2.

Fig. 13 Typical Clad-Core Bond Interface After HIP Bonding at 840°C for Three Hours

Fig. 14a The Power Density Distribution in the Booster Target

Fig. 14b Axial Centerline Profiles of the Internal Heat Generation in the Target Disks Due to Fission and Spallation and the Total

Fig. 15 Average Moderator Neutron Scalar Flux Spectra for the Depleted Uranium and the Booster Targets